This project has received funding from the European Union's Seventh Programme for research, technological development and demonstration under grant agreement No [308417]".

New Directions in Seismic Hazard Assessment through Focused Earth Observation in the Marmara Supersite

Grant Agreement Number: 308417
co-funded by the European Commission within the Seventh Framework Programme
THEME [ENV.2012.6.4-2]
[Long-term monitoring experiment in geologically active regions of Europe prone to natural hazards: the Supersite concept]

D5.4

Near-real time estimation of most relevant earthquake source parameters

Project Start Date	2012 November 1
Project Duration	36 months
Project Coordinator /Organization	Nurcan Meral Özel / KOERI
Work Package Number	WP5
Deliverable Name/ Number	Near-real time estimation of most relevant earthquake source parameters/D5.4
Due Date Of Deliverable	30 April 2015
Actual Submission Date	11 may 2015
Organization/Author (s)	INGV, GFZ, BRGM/ Cirella A., Piatanesi A.,Diao F., Wang R., Aochi H.

Dissemination Level		
PU	Public	
PP	Restricted to other programme participants (including the Commission)	
RE	Restricted to a group specified by the consortium (including the Commission)	
CO	Confidential, only for members of the consortium (including the Commission)	

TABLE OF CONTENTS

1. Introduction

The main goal of this deliverable was the rapid determination of the most relevant earthquake source parameters, with special focus on their finite-fault characteristics, in case of large earthquakes in the Marmara region. To this goal we performed a blind test for kinematic source inversion. BRGM research group generated a synthetic dataset, by considering near-field strong-motion and high-rate GPS data, obtained by dynamic modelling of a single earthquake scenario; and provided these synthetics to the other teams (GFZ, INGV), to invert for the rupture process, by using the different codes, described in deliverable D5.3. This approach allowed us to assess the resolution and efficiency of the different inversion techniques, also in terms of the execution quickness, in the Marmara Sea configuration. GFZ' team performed an additional test, for near real-time kinematic inversions; the related results are described in Section 2.2.3.

2. Blind test

2.1 Description of blind test

In order to carry out the realistic inversion in this region, we provide a synthetic, but more probable scenario, dynamically simulated taking into account of the fault geometry, stress and friction condition. We use one of the scenarios of Mw7.04 from Aochi and Ulrich (BSSA, 2015; LP fault model, T = 0.66, hypocenter location at Center; See Figure 1). The rupture propagates unilaterally to the east. The slip distribution remains relatively simple (briefly one big asperity, illustrated again in Figure 2), but rupture time and slip time function are not imposed. The fault geometry used here is not a single plane fault, but a geometrically irregular fault. All these dynamic factors might have made the wave radiation complex. The ground motion is calculated in the 3D structure model (See D5.3) under the same situations.

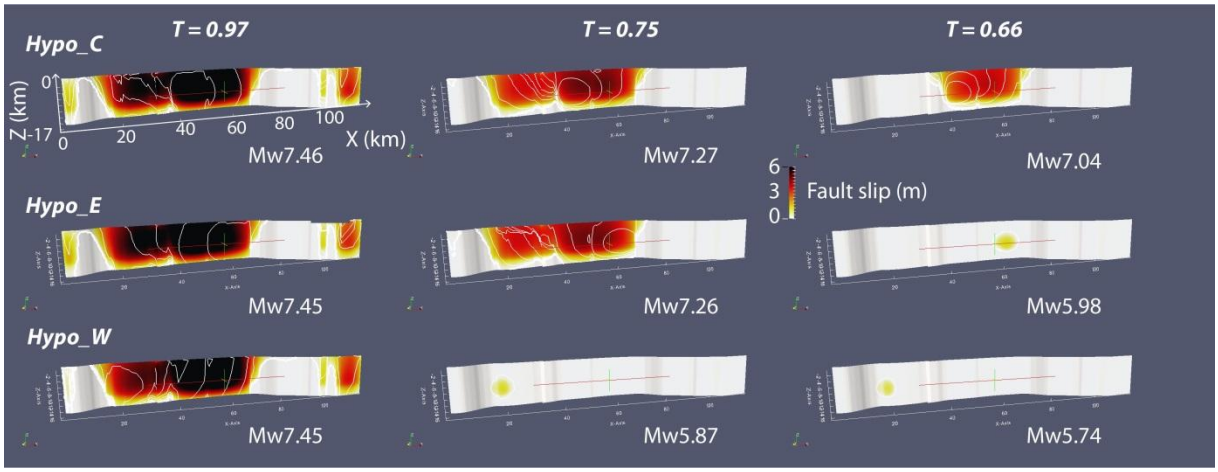

Figure 1. A set of the dynamic rupture simulations from Aochi & Ulrich (BSSA, 2015). The scenario used for the blind test corresponds to the case at the upper-right corner.

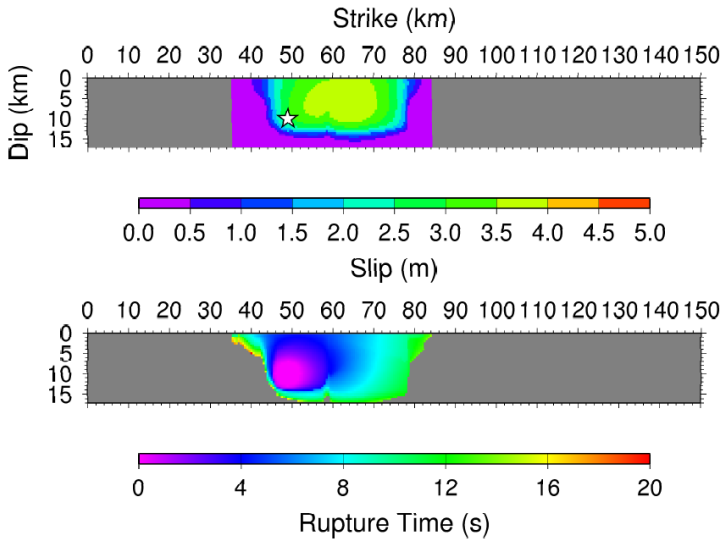

Figure 2. Slip distribution (top) and rupture time (bottom) from the dynamic rupture simulation, projected on a plane fault.

The data set of the same 47 receivers can be downloaded from http://aochi.hideo.perso.neuf.fr/marmara/ (Scenario 1). However for the purpose of blind test, the above information was not informed to the participants before their inversion. Only the following information is provided. Thus, estimating a reasonable magnitude is also an objective of the inversion here.

Informed Parameter	Quantity
Hypocenter	28.5274°E, 40.8717°N, 9.75 km depth
Rupture	It seems that the main Central Marmara part of the North Anatolian fault takes place an earthquake. No fault geometry is given but the same fault orientation as the checker-board test is inferred.

2.2 GFZ' team results

2.2.1 Geometrical setting- Fault parametrization - Data processing

We used a rectangular fault plane (80 km × 24 km) that constructed based on the focal mechanism (strike=86°, dip=90°). This fault geometry was discretized to 120 subfaults of 4 km × 4 km size, each being treated as a point source. We fixed the rake angle to be 180°. The data was processed using the same approach as mentioned in D5.3 (Section 2.2.1). We did not constraint the rupture velocity, rise time and the shape of the rise time function in the inversion. The corner frequency used for the blind test is 0.10 Hz.

2.2.2 Results

The inverted source model of the blind test is shown in Fig. 3. The rupture model suggests that the moment magnitude is 7.03 and the rupture process last for 20 second. With a rupture scale of ~ 35 km and a slip maximum of 5 m, the fault slip are mostly located at depths less than 16 km. The data fit is shown in Fig. 4, from which we found that the large misfit mainly lies at the high frequency components that induced by 3D wave propagation effect.

The computation time used for inversion of the rupture models is **120 seconds** with a PC (Intel(R) Core (TM) i7-3770 CPU @3.4G Hz, 32 GB RAM).

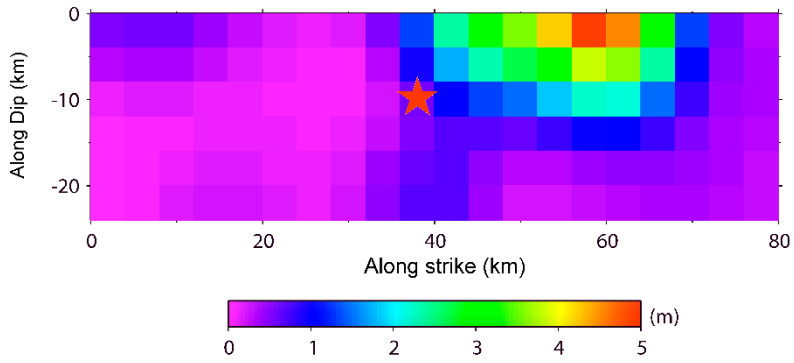

Figure 3. Rupture model inverted based on synthetic datasets that simulated from 3D earth structure.

2.2.3 Test for near real-time kinematic inversions

For purposes of tsunami early warning and earthquake rapid response, time-dependent finite-fault source inversions are of great importance. Here we address the question how fast such source models can be obtained theoretically for the Marmara Sea region. The time delay for kinematic source inversion addressed here is not the computation time but the time for seismic wave propagation from the source to the seismic stations.

For this purpose, we adopt the IDS inversion scheme and predetermined fault geometry (Fig. 5) for a real-time data processing. Here the term “real-time” means using only the data which become available. We used a different earthquake scenario with moment magnitude of 7.19, which is the scenario 2 from Aochi H. (http://aochi.hideo.perso.neuf.fr/marmara/). We assume that large earthquakes (M 7+) can only occurred on the main Marmara Sea fault. For this reason, all major seismogenic faults in the Marmara Sea region identified by Armijo et al. (2005) were assumed to have the same potential to nuclear large-scale earthquakes in the inversion. The right-lateral strike-slip mechanism is assigned uniformly according to various geological and geomechanical investigations (Armijo et al., 2005; Hergert et al.,

2011). These faults are then divided into 4 km × 4 km subfaults. Each subfault is allowed to rupture at any time after the origin of the event.

For the real-time inversions, we repeat the inversion each 10 s. The results are the time-dependent slip distributions shown in Fig. 5 and Fig. 6. From the real-time magnitude curve, the final moment magnitude (Mw 7.19) of the utilized scenario earthquake seems to be available at about 30 s after the true event occurrence (Fig. 6). However, it is partly contributed by the numerical noises on neighboring non-causal faults. Figure 5 shows the slip distribution on the causal fault stabilizes not earlier than 50 s after the event occurrence, but the causal fault can be recognized already from 20-30 s. Note that the rupture duration of the earthquake is 20 s. Thus, the actual time delay for getting the final source model is at least 30 s, a large part of which is caused by the travel times of S waves to the seismic stations.

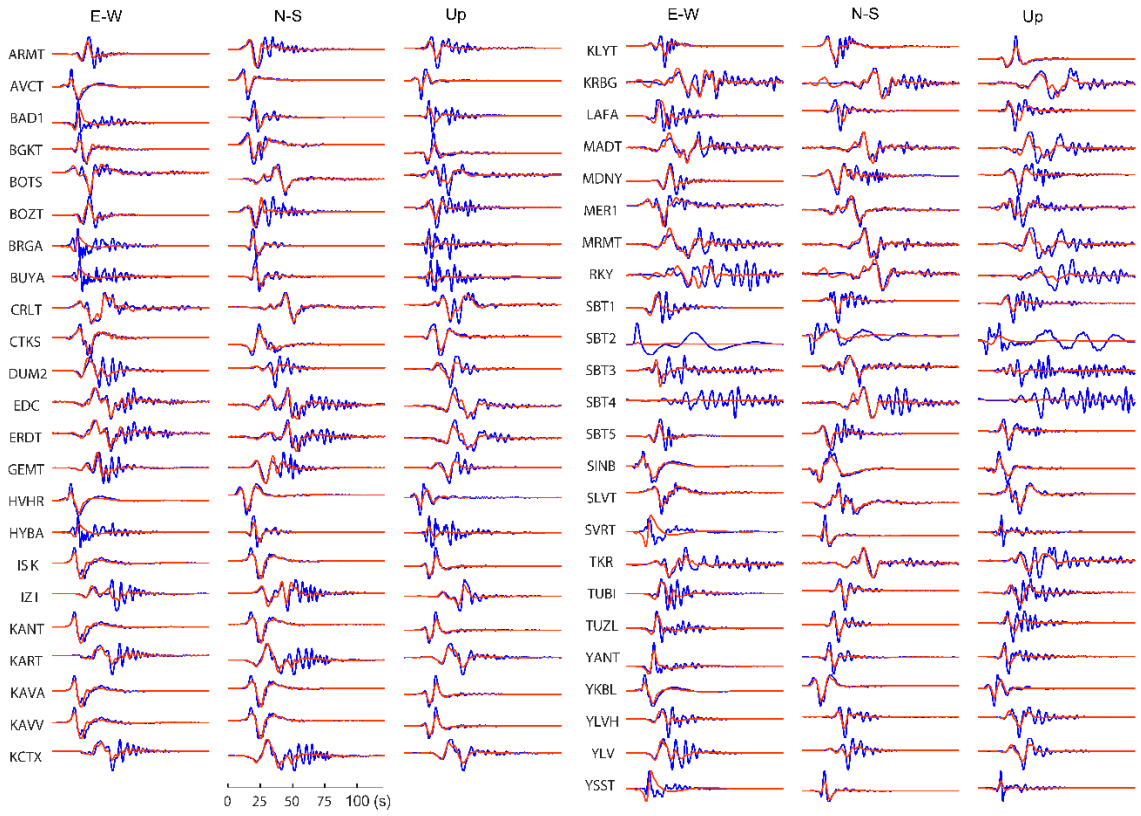

Figure 4. Waveform comparison between synthetic (blue) and inverted (red) velocity seismograms for the rupture model shown in Fig. 3.

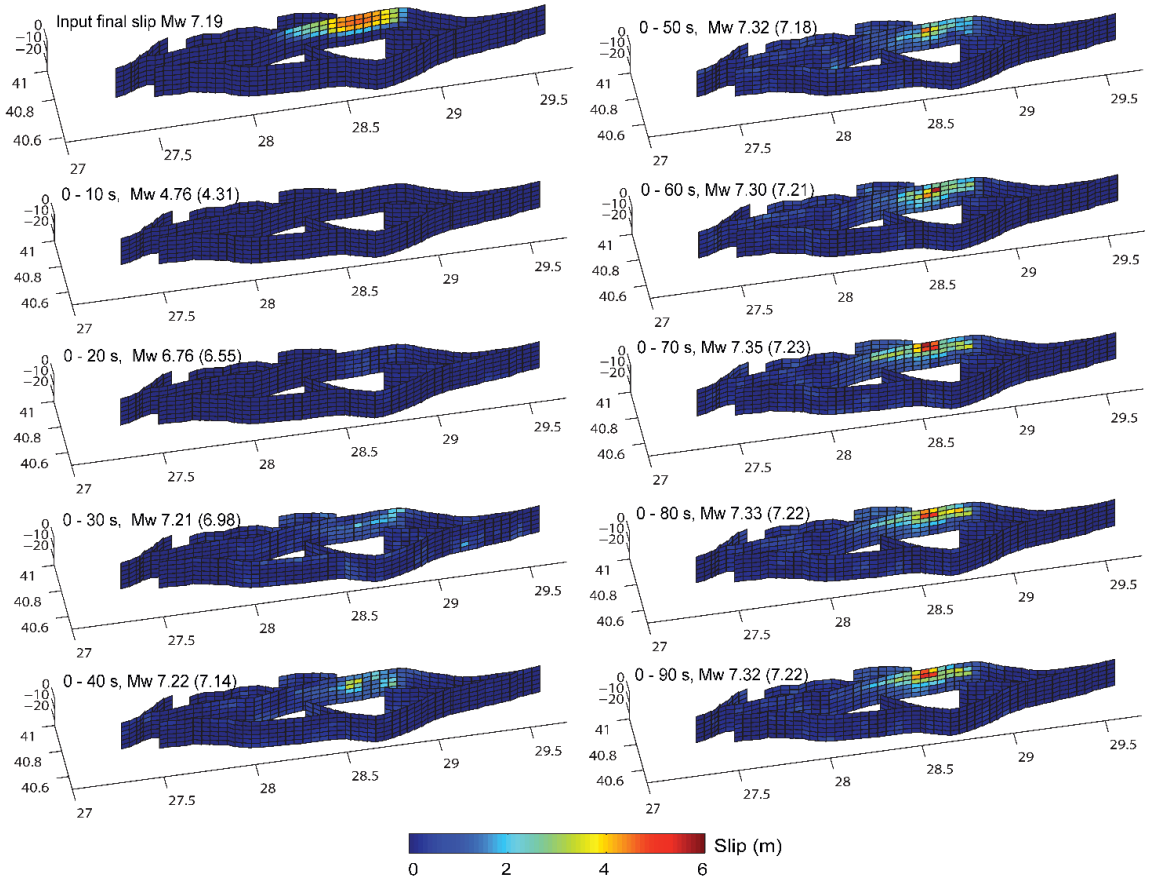

Figure 5. Comparison between the input (top left) and real-time reconstructed slip models. The moment magnitudes outside the brackets are inferred from the seismic moment distributed on the whole fault system, while that in the brackets corresponds to seismic moment located on the main rupture fault.

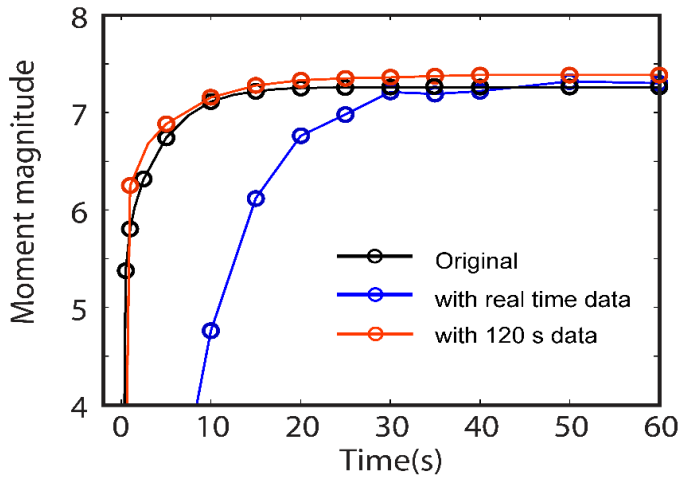

Figure 6. Moment magnitude curves obtained by the retrospective (red) and real-time reconstruction (blue) in comparison with the input one (black).

2.3 INGV' TEAM RESULTS

2.3.1 Geometrical setting- Fault parametrization - Data processing

We used the 47 synthetic seismograms provided for Scenario1 (http://aochi.hideo.perso.neuf.fr/marmara/). Original ground velocity time histories are band-pass filtered in two different frequency ranges; between 0.01 and 0.5 Hz and between 0.01 and 0.25Hz, by using a two-pole and two-pass Butterworth filter. We invert 60 seconds of each waveform, including body and surface waves. We assumed a fault plane consistent with the hypocentre location and the focal mechanisms given for the Central Marmara segment (Scenario1 strike: 86°; dip=90°). The fault plane is 95 km long and 24 km width, along strike and down-dip direction, respectively. We invert simultaneously for all the parameters at nodal points equally spaced (4.5 km) along strike and dip directions. During the inversion, we fix a given range of variability for each model parameter. In particular, in this study we adopt the following variability intervals: peak slip velocity values can range between 0 and 7.0 m/s at 0.25 m/s interval; the rise time between 1.0 and 4 sec at 0.25 sec interval and the rupture time at each grid node is constrained by the arrival time from the hypocentre of a rupture front having a speed comprised between 2 and 4 km/s. Rake angle is fixed to 180°. In this study, the adopted source time function is a regularized Yoffe function having a constant time to peak slip velocity (T_{acc}) equal to 0.225 sec (Tinti et al., 2005). We adopted the inversion technique described in Section 2.3.1 (D5.3).

2.3.2 Results

We performed six different inversions:

1. by inverting for peak slip velocity, in the frequency range 0.01-0.25 Hz. Rise time, rake angle and rupture velocity are fixed; CPU=13minutes; (results are referred as case '1par0.25Hz');
2. by inverting for peak slip velocity, in the frequency range 0.01-0.5 Hz. Rise time, rake angle and rupture velocity are fixed; CPU=1h; (results are referred as case '1par0.5Hz');
3. by inverting for peak slip velocity and rise time, in the frequency range 0.01-0.25 Hz. Rake angle and rupture velocity are fixed; CPU=2h; (results are referred as case '2par0.25Hz');
4. by inverting for peak slip velocity and rise time, in the frequency range 0.01-0.5 Hz. Rake angle and rupture velocity are fixed; CPU=6h ; (results are referred as case '2par0.5Hz');
5. by inverting for peak slip velocity, rise time and rupture time, in the frequency range 0.01-0.25 Hz. Rake angle is fixed to 180°; CPU=3.30h ; (results are referred as case 'Allpar0.25Hz');

6. by inverting for peak slip velocity, rise time and rupture time, in the frequency range 0.01-0.5 Hz. Rake angle is fixed to 180°; CPU= 8.30h; (results are referred as case ‘Allpar0.5Hz’).

For each inversion we show (see Figures 7-9-11-13-15-17) the retrieved rupture model, given in terms of rise time, slip, peak slip velocity and rupture times distribution (depending on the set of inverted kinematic parameters) on the fault plane, and the corresponding comparison between synthetic (blue lines) and inverted (red lines) velocity time histories (see Figures 8-10-12-14-16-18).

Case: 1par0.25Hz

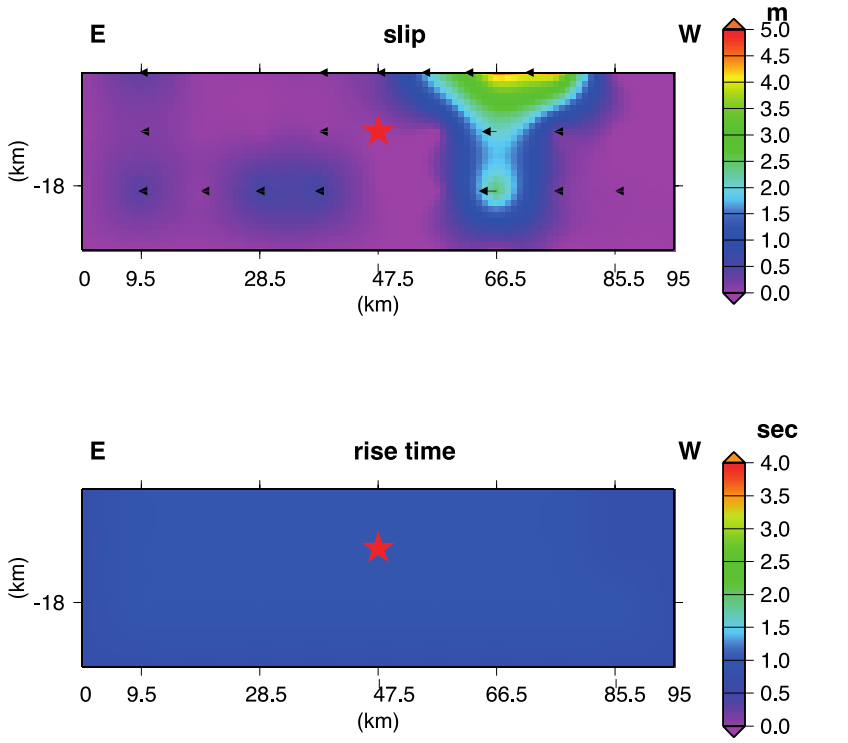

Figure7. Retrieved rupture model, in terms of slip and rise time distribution (upper and bottom panel, respectively), obtained by inverting for peak slip velocity, in the frequency band 0.01-0.25Hz.

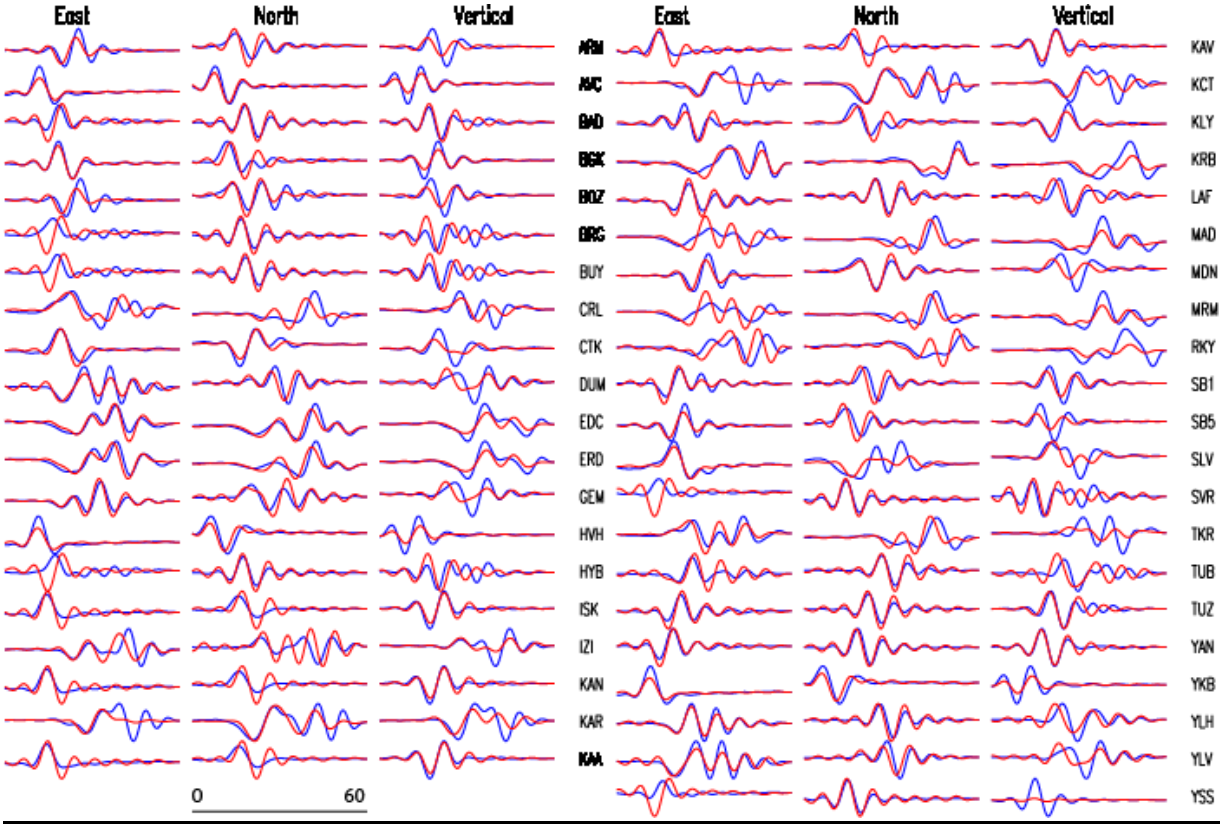

Figure8. Misfit between synthetic ground velocities (blue lines) with those computed from the inverted rupture model displayed in Figure7 (red lines).

Case: 1par0.5Hz

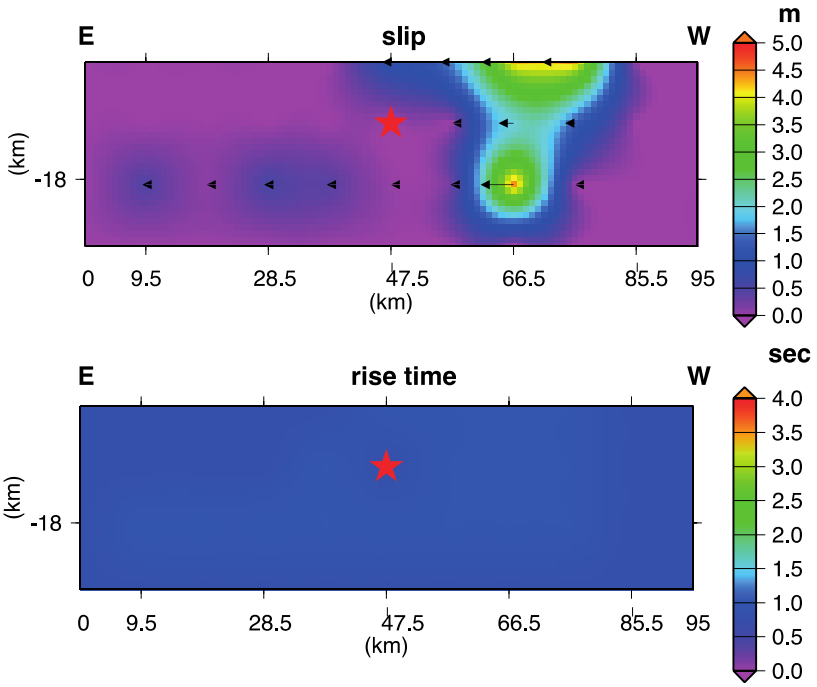

Figure9. Retrieved rupture model, in terms of slip and rise time distribution (upper and bottom panel, respectively), obtained by inverting for peak slip velocity, in the frequency band 0.01-0.5Hz.

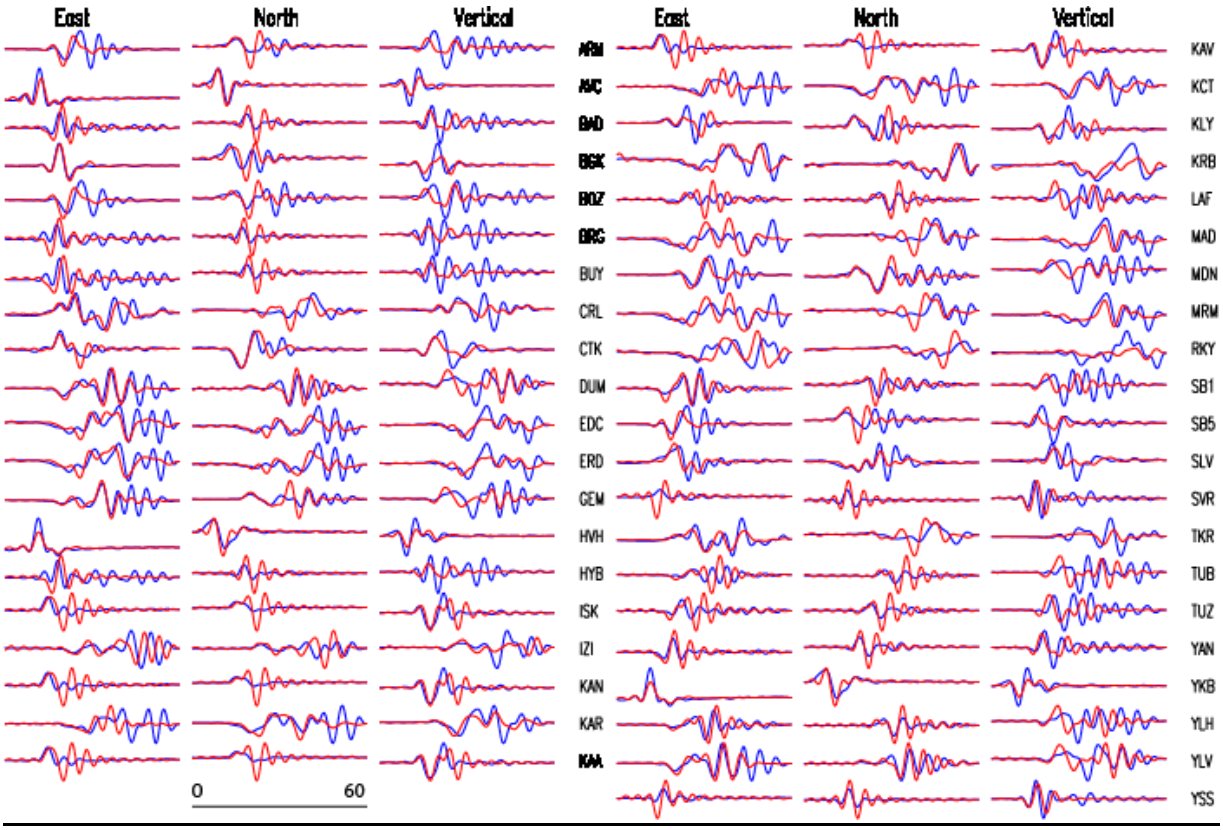

Figure10. Misfit between synthetic ground velocities (blue lines) with those computed from the inverted rupture model displayed in Figure9 (red lines).

Case: 2par0.25H

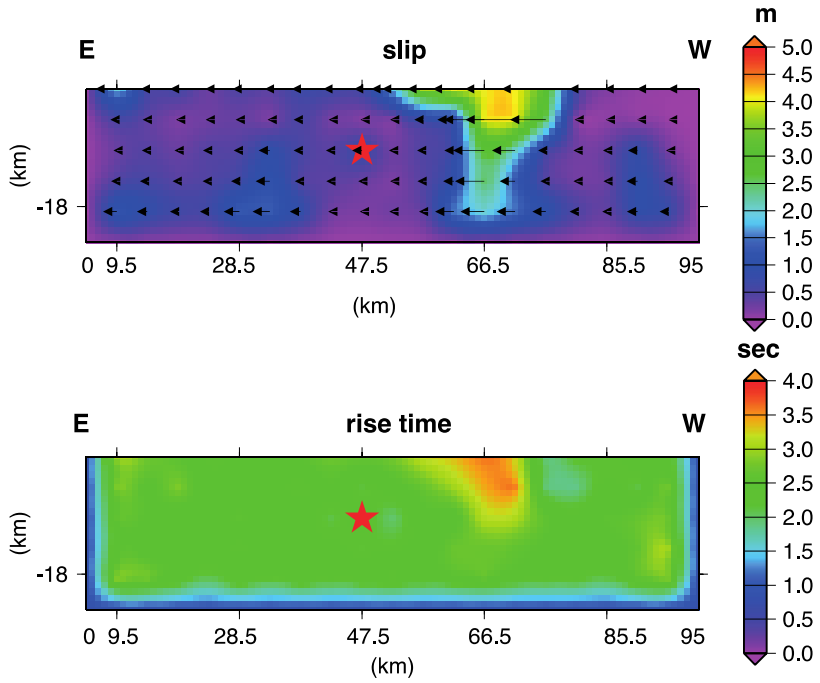

Figure11. Retrieved rupture model, in terms of slip and rise time distribution (upper and bottom panel, respectively), obtained by inverting for peak slip velocity and rise time, in the frequency band 0.01-0.25Hz.

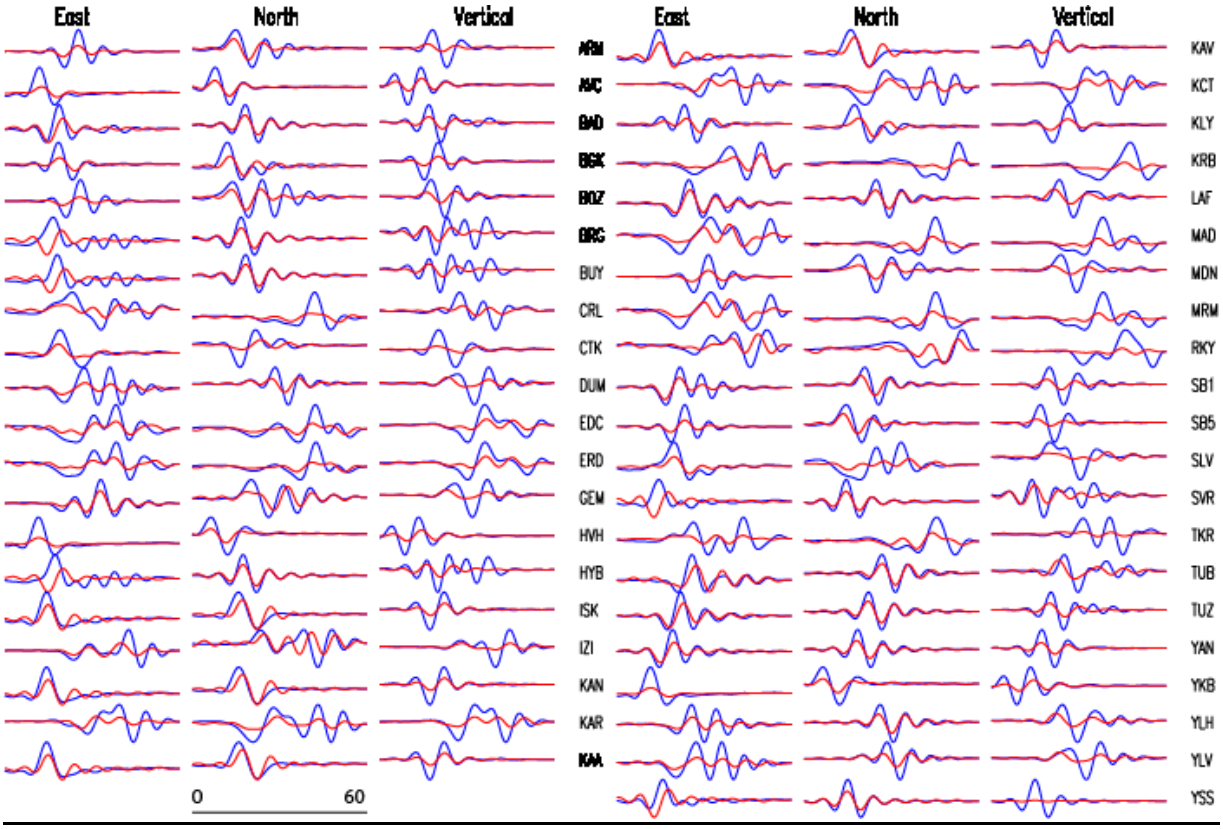

Figure12. Misfit between synthetic ground velocities (blue lines) with those computed from the inverted rupture model displayed in Figure11 (red lines).

Case: 2par0.5Hz

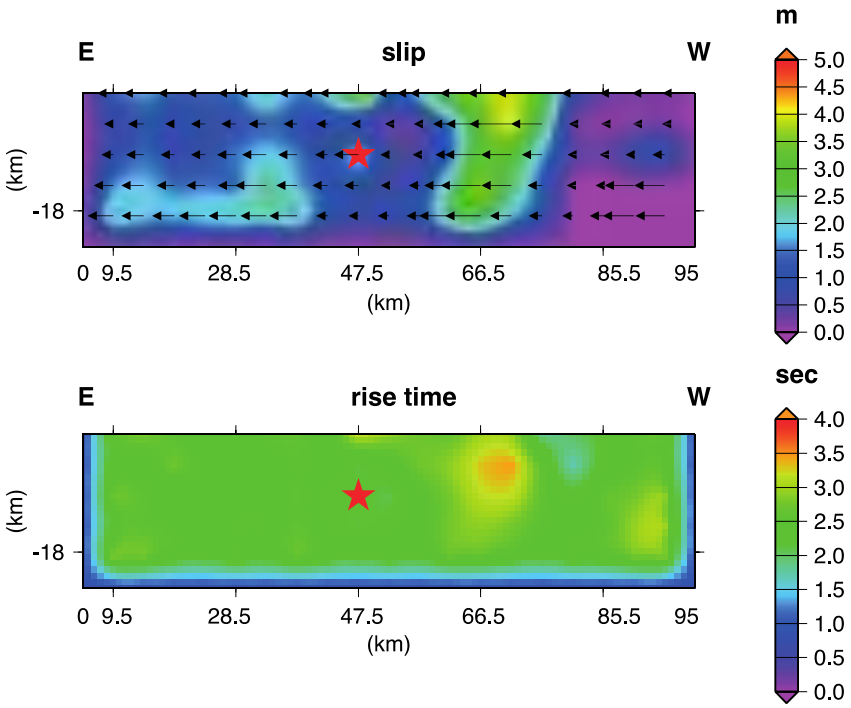

Figure13. Retrieved rupture model, in terms of slip and rise time distribution (upper and bottom panel, respectively), obtained by inverting for peak slip velocity and rise time, in the frequency band 0.01-0.5Hz.

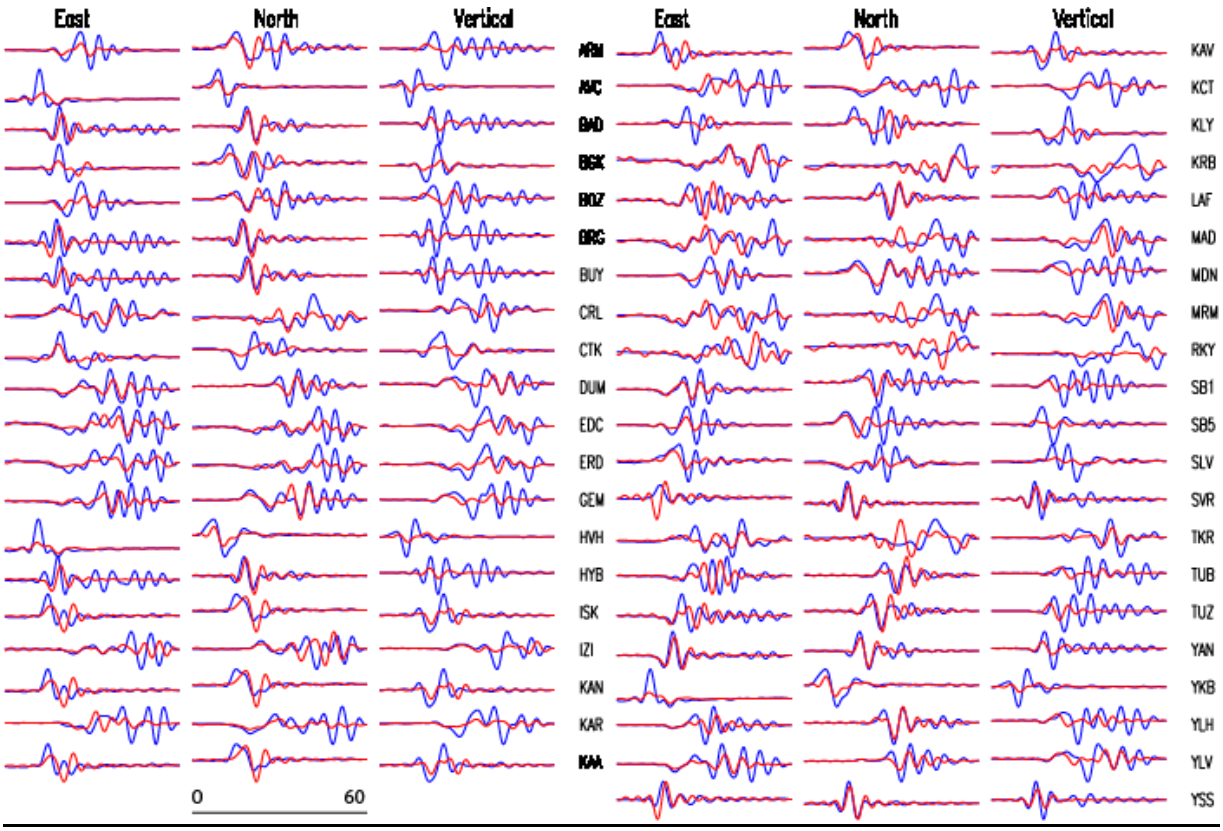

Figure14. Misfit between synthetic ground velocities (blue lines) with those computed from the inverted rupture model displayed in Figure13 (red lines).

Case: Allpar0.25Hz

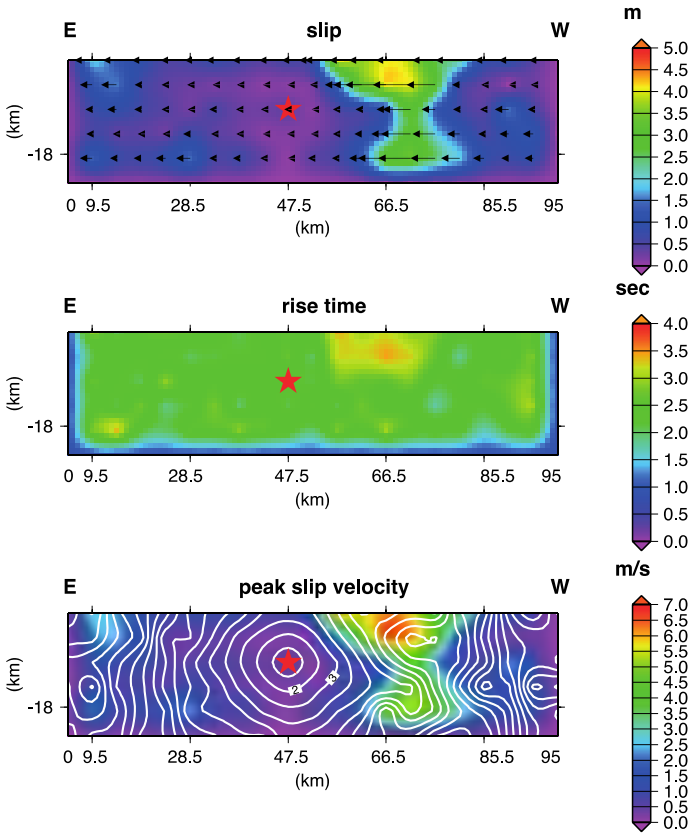

Figure15. Retrieved rupture model, in terms of slip, rise time, peak slip velocity and rupture time distribution (upper, middle, and bottom panel, respectively), obtained by inverting for peak slip velocity, rise time and rupture time, in the frequency band 0.01-0.25Hz. White contours in bottom panel show the retrieved rupture times.

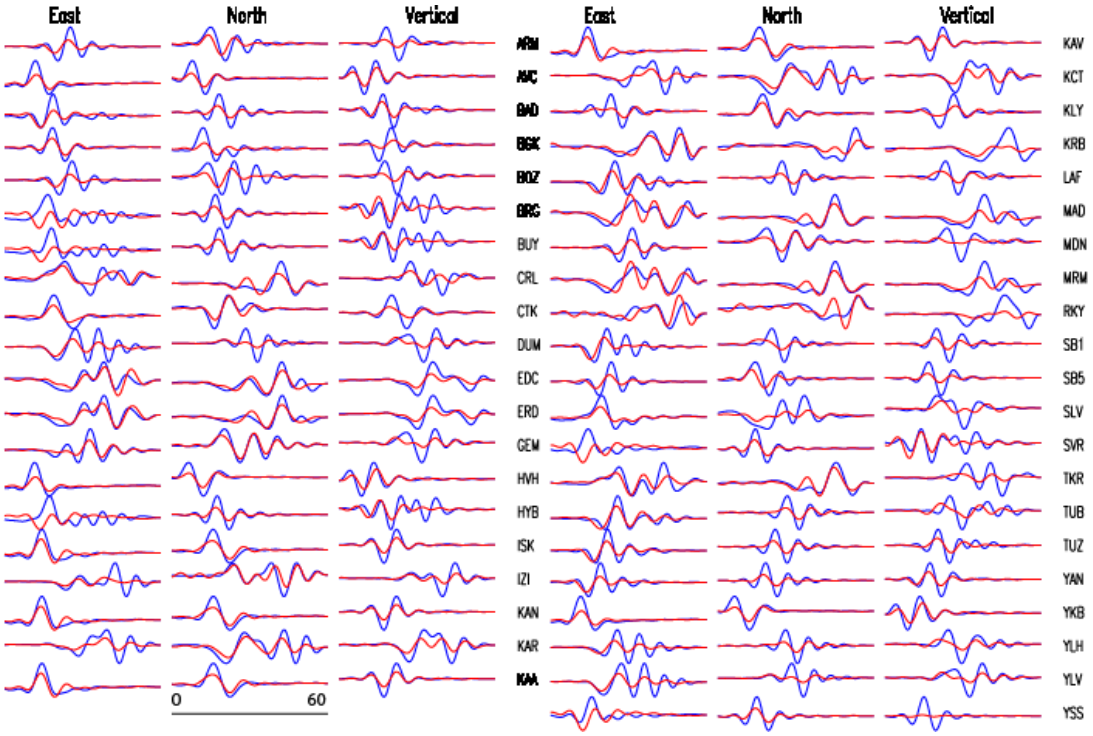

Figure16. Misfit between synthetic ground velocities (blue lines) with those computed from the inverted rupture model displayed in Figure15 (red lines).

Case: Allpar0.5Hz

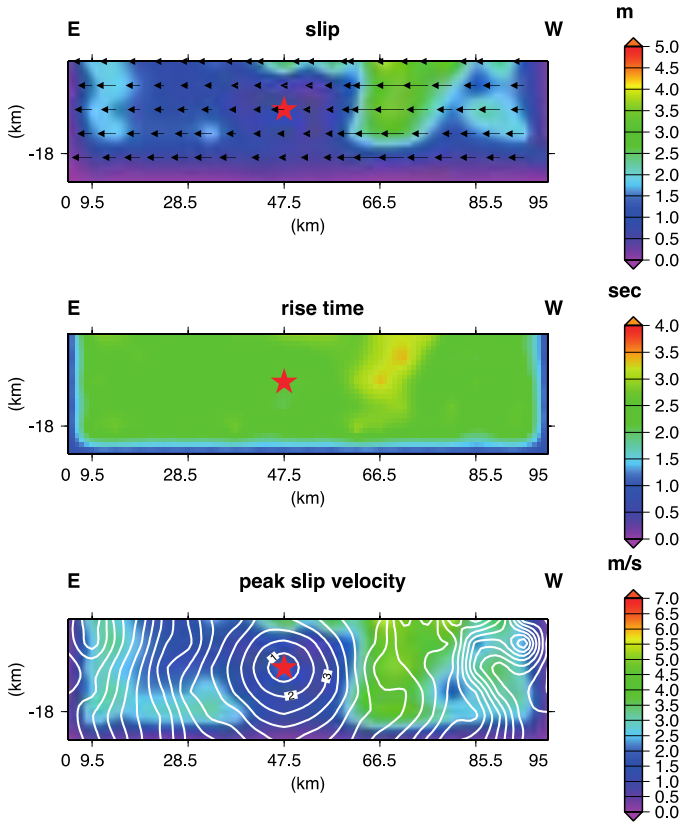

Figure17. Retrieved rupture model, in terms of slip, rise time, peak slip velocity and rupture time distribution (upper, middle, and bottom panel, respectively), obtained by inverting for peak slip velocity, rise time and rupture time, in the frequency band 0.01-0.5Hz. White contours in bottom panel show the retrieved rupture times.

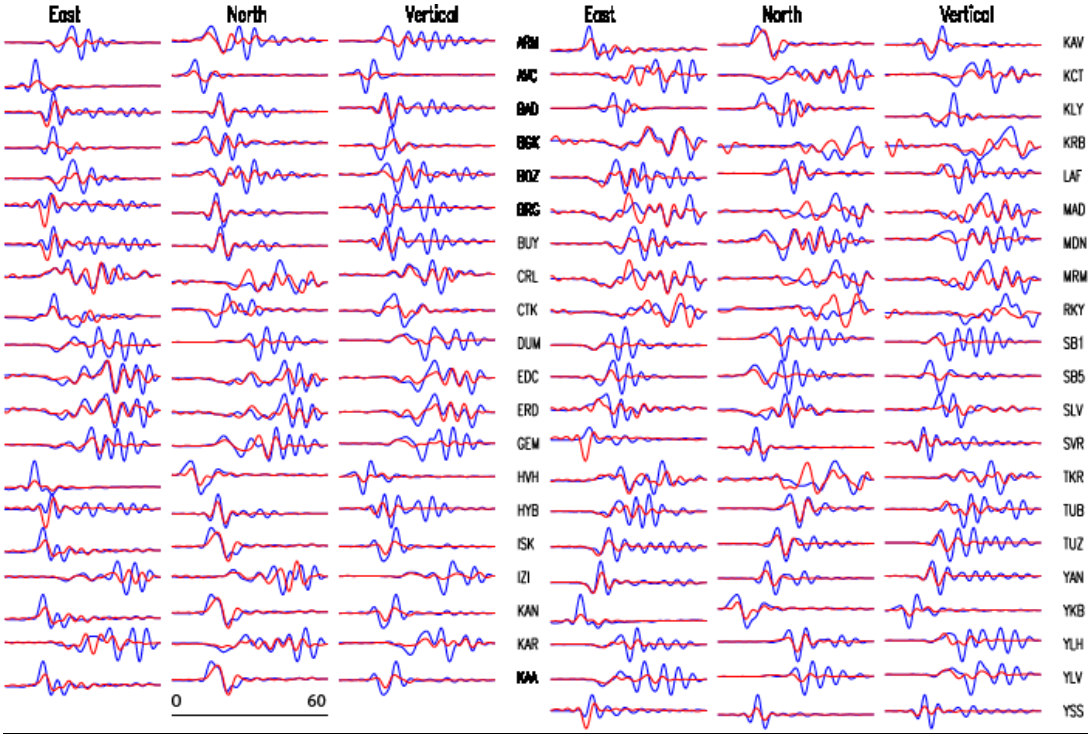

Figure18. Misfit between synthetic ground velocities (blue lines) with those computed from the inverted rupture model displayed in Figure17 (red lines).

All the retrieved rupture models are characterized by a main patch with a maximum slip value of 4 m that extends from the right-upper fault plane border down to a depth of 14 km. The associated moment magnitudes are all around 7 (see fourth and seventh column in Table1). The total duration of the rupture is about 20s; and the slip asperity is characterized by rise time of about 2-3.5 s (Figures 15-17).
Table1 also shows, for each performed inversion, the corresponding waveform' cost function (second and fifth column in Table1) and the computation time (CPU), (third and sixth column in Table1). All inversions were done with a PC (Intel Xeon E5-2680 processor running CPU @2.7GHz, 128 GB RAM). As we can see, our code is able to retrieve a good rupture model (cost=0.35) in 13minutes. We consider this result a rapid and reliable estimation of the main rupture process' features.

Table1. CPU, waveform Cost function, Moment Magnitude values

	0.01 – 0.25 Hz			0.01 – 0.5 Hz		
	cost	CPU	Mw	cost	CPU	Mw
Allpar	0.23	3.30h	7.10	0.42	8.30h	7.07
2par	0.29	2.00h	7.08	0.56	6.00h	7.06
1par	0.35	13min	7.01	0.50	1.00h	7.00

3. Conclusions

Information about the extended source properties are needed for performing the ground motion simulation associated to the earthquake rupture on the causative fault. The main goal of this task was the fast determination of the earthquake source, with special focus on its finite-fault characteristics. The obtained result, for the blind test, show that, by inverting near-field strong-motion and high-rate GPS data in the Marmara Sea we are able to provide a rapid (CPU between 2 and 13 minutes) and reliable reconstruction of the rupture process of large earthquakes, by retrieving the most relevant earthquake source parameters. These analyses can be done in near real time and are particularly suited for capturing near-source large earthquakes. The proposed approach represents a helpful tool to improve rapid ground-motion simulations in case of large earthquakes in the Marmara region. Moreover, according to the test results, performed by the GFZ team, near real-time source characterization of large-scale earthquakes (Mw $\geq$ 7)

under the Marmara Sea is feasible. Providing the real-time data acquisition for the current network and a good database of the active fault system, all key source parameters that are relevant for purpose of the rapid hazard assessment can be estimated without substantial uncertainties. The theoretical time delay between what can be resolved and what has been really occurred on the earthquake source is in the order of 10-15 s. The cause of this time delay is mainly physical, namely by the S wave propagation from the source to the network. In practice, a slightly larger time delay should be considered because of the time to be required additionally for the data transmission and inversion. The latter, however, can be generally reduced to a few seconds through parallelization of the IDS inversion technique.

References

Aochi, H. and T. Ulrich, A probable earthquake scenario near Istanbul determined from dynamic simulations, Bull. Seism. Soc. Am. , 105, doi:10.1785/0120140283, 2015.

Armijo, R. & 21 others, 2005. Submarine fault scarps in the Sea of Marmara pull-apart (North Anatolian Fault): Implications for seismic hazard in Istanbul, *Geochem. Geophys. Geosyst*., 6, Q06009, doi:10.1029/2004GC000896.

Hergert, T., Heidbach, O., Bécel, A. & Laigle, M., 2011. Geomechanical model of the Marmara Sea region - I. 3-D contemporary kinematics, *Geophys. J. Int*., 185, 1073-1089, doi:10.1111/1365-246X.2011.04991.x.

Tinti, E., E. Fukuyama, A. Piatanesi and M. Cocco (2005a), A kinematic source time function compatible with earthquake dynamics, *Bull. Seismol. Soc. Am*., 95(4), 1211-1223, doi:10.1785/0120040177.